Adsorption of Cyclopentene on Pt(111) and Ordered Pt_nSn/Pt(111) Surface Alloys

Conrad Becker,*,† Francoise Delbecq,‡ Jürgen Breitbach,† Guido Hamm,† Dieter Franke,† Franziska Jäger,† and Klaus Wandelt†

Institut für Physikalische und Theoretische Chemie, Universität Bonn, Wegelerstrasse 12, 53115 Bonn, Germany, and Ecole Normale Supérieure de Lyon, UMR CNRS 5182, 46 Allée d'Italie, 69364 Lyon Cedex 07, France

Received: June 25, 2004; In Final Form: September 22, 2004

The adsorption of cyclopentene (C_5H_8) on Pt(111) and the two ordered Pt_3Sn/Pt(111) and Pt_2Sn/Pt(111) surface alloys has been investigated experimentally using high-resolution electron energy loss spectroscopy, ultraviolet photoelectron spectroscopy, low-energy electron diffraction, and temperature-programmed desorption as well as theoretically by ab initio density functional theory (DFT) calculations. On the Pt(111) and the respective surface alloys, a di-σ bonding of cyclopentene has been found both experimentally as well as in the DFT calculations. Even though the bonding mechanism on Pt(111) and the two surface alloys is very similar, large differences in the bond energy and the thermal stability of the cyclopentene have been detected. On Pt(111), part of the C_5H_8 desorbs intact at ~280 K whereas the remaining amount is converted to C_5H_5. This species completely dehydrogenates to carbon upon heating above 450 K. On the surface alloys, the temperature of desorption is reduced to 244 K (Pt_3Sn) and 198 K (Pt_2Sn), respectively, and no dehydrogenation is detected. The influence of the aliphatic ring on the interaction between the olefinic bond and the substrate is weak even though an interaction of the β-hydrogen with the surface atoms has been found experimentally and theoretically for cyclopentene on Pt(111) and on the Pt_3Sn/Pt(111) surface alloy.

Introduction

Sachtler pointed out in the early 1970s that the reactivity of alloy surfaces can vary significantly from that of pure metals.[1] He considered that two major effects play an important role for the reactivity of alloy surfaces. The so-called *ligand effect*, which is due to the changes of the electronic structure of the constituents of an alloy caused by the redistribution of charge between them, will inevitably change the interaction with an adsorbate. The steric constraints imposed by particular adsorption sites, disregarding electronic effects, are subsumed under the so-called *ensemble effect*. Both effects are of course idealized limiting cases, which in general are not encountered on real surfaces. Nevertheless, they provide a helpful concept for the discussion of the effects found for the adsorption of surface alloys.

Good candidates for adsorption experiments in light of the above seem to be Pt−Sn surface alloys. Although the Sn atoms are believed to act mainly as site blockers,[2,3] adsorption experiments[3] and scanning tunneling microscopy (STM) images of the alloy surfaces[4] indicate a slight modification of the electronic structure of the surface, which is consistent with theoretical calculations showing a hybridization between Pt d- and Sn p-electrons and a reduction of the local density of states (LDOS) at the Fermi level.[5,6] Furthermore, Pt−Sn surface alloys can be easily prepared by annealing of a Sn-covered Pt(111) surface. The resulting surface alloys exhibit, depending on the annealing temperature, a (2×2) or $(\sqrt{3} \times \sqrt{3})R30°$ low-energy electron diffraction (LEED) pattern corresponding to a surface composition of Pt_3Sn and Pt_2Sn, respectively.[2,7−10]

Extensive studies of the adsorption of hydrocarbons on Pt_nSn/Pt(111) by Koel and co-workers showed a reduced reactivity of the surface alloys for dehydrogenation.[7,11−18] The completely suppressed dehydrogenation of ethylene on the surface alloys was claimed to result from missing adjacent platinum 3-fold hollow sites for accommodating the decomposition products, namely, ethylidine.[3,11]

The adsorption of cyclopentene on Pt(111) was considered for the first time by Avery using temperature-programmed desorption (TPD) and high-resolution electron energy loss spectroscopy (HREELS).[1,2] According to Avery, at 100 K cyclopentene is di-σ-bonded to the surface. Upon heating to 250 K, the molecules decompose to a new species identified as cyclopentadienyl (C_5H_5). Later Avery's observations were confirmed with X-ray photoelectron spectroscopy (XPS), bismuth postdosing TPD,[3] and infrared reflection−absorption spectroscopy (IRAS).[14] In contrast to these measurements, semiempirical calculations by Brizuela indicated only a physisorbed species populating 3-fold hollow sites.[13] An exact experimental and theoretical determination of the adsorption site of Pt(111) is, thus, still missing. The adsorption of cyclopentene on the Pt_nSn/Pt(111) surface alloys has not been studied to date.

The aim of the present work was, thus, twofold. First, the adsorption of cyclopentene on Pt(111) has been reinvestigated both experimentally and theoretically in order to determine the exact bonding mechanism and geometry as well as the origin of the dehydrogenation. These data are indispensable as a reference framework for the subsequent study of the cyclopentene adsorption on the Pt_nSn surface alloys. Furthermore, the role of the aliphatic ring for the bonding has been investigated, which is of particular interest when comparing the results to those obtained for ethene adsorption on the same surfaces. Second, the adsorption of cyclopentene on the alloys has been

* Corresponding author. Fax: +49 228 73 2551. E-mail: conrad.becker@uni-bonn.de.
† Universität Bonn.
‡ Ecole Normale Supérieure de Lyon.

10.1021/jp047228j CCC: $27.50
Published on Web 11/12/2004

studied in order to determine the influence of the tin on the adsorption strength, the adsorption geometry, and the dehydrogenation.

Experimental Details

The experiments were performed in two different ultrahigh vacuum chambers operated at base pressures of $\approx 1 \times 10^{-8}$ Pa. One was equipped with a high-resolution electron energy loss spectrometer (VSW IB2000), an Auger electron spectrometer, back-view LEED optics, and a quadrupole mass spectrometer for thermal desorption experiments (TPD); the second one was equipped for Auger electron spectroscopy (AES), LEED, TPD, and ultraviolet photoelectron spectroscopy (UPS).

For the experiments a disk-shaped Pt(111) sample of 7 mm diameter (MaTeck, Jülich) was used, which was mounted between tantalum wires wedged into grooves in the sides of the crystal. Heating was performed by direct current through these wires. In the HREELS chamber, cooling was provided by an LN_2 reservoir, which was directly connected to the sample holder. In the UPS chamber, the sample holder was connect to a closed-cycle He refrigerator, which allowed for sample temperatures down to 55 K. Clean Pt(111) surfaces were obtained by cycles of Ar^+ ion sputtering (10 min, 1 keV, 2.5 μA) at 900 K and subsequent annealing at 1100 K for 2 min. The cleanliness of the Pt(111) surface was monitored by AES and HREELS.

The TPD experiments were performed using a constant heating rate of 2 K s^{-1}, which was controlled by a Eurotherm 2408 temperature controller. Up to four different masses were detected concurrently. The HREELS spectrometer was run at a resolution of 3−4 meV and a primary energy of 5 eV. Spectra were recorded in specular geometry at a scattering angle of 60° relative to the surface normal.

An Al_2O_3 crucible was used for the evaporation of Sn, which was wrapped by a tungsten filament and temperature controlled by a thermocouple of type K. To ensure a constant Sn flux, the evaporator was operated at a temperature of 1300 K, which yielded a deposition rate of ~0.001 ML s^{-1} (ML, monolayer) at a pressure in the 1×10^{-8} Pa range.

The preparation of the Pt−Sn surface alloys was monitored using AES and LEED and has been described in detail in ref 2.

Computational Details

The calculations were performed with the Vienna ab initio Simulation Package (VASP).[19−21] This program performs periodic density functional theory (DFT) calculations using a plane-wave basis set and the PAW method. The PAW method is a frozen core method, which uses the exact valence wave functions instead of pseudopotentials.[22] The generalized gradient approximation (GGA) level was used with the functional of Perdew and Wang 91.[23]

The surfaces were modeled by periodic four-layer slabs with adsorption on one side of the slab. For the alloys, only the first layer contains Sn atoms in a stoichiometry Pt_3Sn for the (2×2) structure and Pt_2Sn for the $(\sqrt{3} \times \sqrt{3})R30°$ one. Each slab is separated from its periodic image in the *z*-direction by a vacuum space corresponding to five layers (11.5 Å). One molecule is adsorbed per unit cell. For all structures, the geometry optimization included all degrees of freedom of the adsorbed molecule and of the two uppermost metal layers.

For the frozen part of the slab, the same metal interatomic distance (2.82 Å) was used in the case of pure platinum and in the case of the alloys (optimized from Pt bulk calculations, 2% larger than the experimental value of 2.77 Å). This is justified by the fact that experimentally the lattice parameter is imposed by the underlying Pt bulk and the Sn atoms in the uppermost layer accommodate this constraint by an outward displacement, inducing a Pt−Sn distance of 2.86 Å. The adsorption energy is defined as the difference between the energy of the whole system and that of the bare slab and the isolated adsorbate.

Since the molecules are adsorbed on one side of the slab only, the unit cell has a net dipole and a spurious electrostatic interaction between the slab and its periodic images can modify the total energy. A correction has been applied both on the energy and on the calculated potential, to remove this effect. This correction does not exceed 30 meV for Pt and 60 meV for the alloys.

The HREELS spectra were simulated by calculation of the vibrational frequencies.[24] The technique for calculating these frequencies is based on the numerical calculation of the second derivatives of the potential energy surface within the harmonic approach. The coupling with the surface phonons is neglected. The force constant matrix was built with finite differences of the first derivatives of the total energy by geometrical perturbations of the optimized Cartesian coordinates of the system. The diagonalization of this matrix provides the harmonic molecular frequencies and the associated harmonic normal vibration modes. The intensities of the EELS spectra are estimated by applying the formula given in ref 25 where the intensities are proportional to the square of the dynamic dipole moments (derivatives of the dipole moments with respect to a given normal mode), to a function depending on experimental parameters, and to the inverse of the frequencies.

Results

Adsorption of Cyclopentene on Pt(111). To establish reference data for the investigation of adsorption of cyclopentene on the Pt_nSn/Pt(111) surface alloys, we chose to reinvestigate the adsorption on Pt(111). This approach was also triggered by the fact that a HREEL spectrometer with improved resolution was used and that no valence band photoemission data were published to date. Furthermore, the investigation of the TPD results on all three surfaces allowed us to compare the relative amounts of cyclopentene, which can be chemisorbed on these at saturation coverage.

The TPD spectra of molecular hydrogen ($m/e = 2$) and cyclopentene ($m/e = 67$) from the Pt(111) surface after cyclopentene exposure at 100 K, which are displayed in Figure 1, are in excellent agreement with previous results of Avery[26,27] and Henn et al.[28] They show that the molecular desorption of cyclopentene starts only for exposures above 1.5 langmuir. The spectra are characterized by two maxima at 136 and 280 K, respectively. The peaks can be assigned to desorption from cyclopentene multilayers (136 K) and from the monolayer (280 K) by the help of HREELS (see below). A desorption temperature of 280 K found for the monolayer species can be translated into a desorption energy of 79 kJ mol^{-1} using a Redhead analysis[29] under the assumption of first-order kinetics and a pre-exponential factor of 10^{13} s^{-1}. The desorption spectra of the hydrogen evolution are characterized by the presence of two peaks at roughly 300 K (β_1) and 500 K (β_2). The second peak exhibits a broad tail that extends up to 750 K. When one compares the spectra of hydrogen and cyclopentene at exposures below 1.5 langmuir, it becomes evident that the absence of cyclopentene desorption in this exposure range is caused by the dehydrogenation of the entire quantity of adsorbed cyclo-

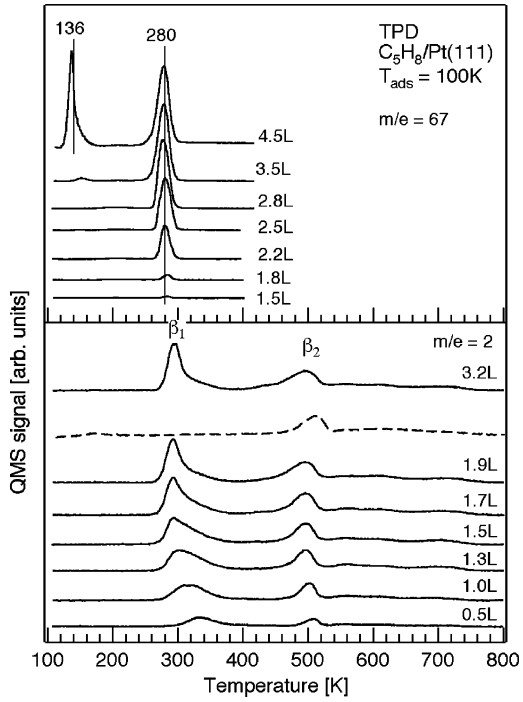

Figure 1. TPD spectra of cyclopentene absorbed on Pt(111) at 100 K. The top graph shows the desorption traces of molecular cyclopentene ($m/e = 67$) for various exposures. At the bottom, the corresponding spectra for reactively formed hydrogen ($m/e = 2$) desorption are shown. The heating rate was 2 K s^{-1} for all spectra. The dashed line in the lower spectra shows the hydrogen evolution from a full monolayer of benzene on the Pt(111) surface for comparison.

pentene. A quantitative analysis of the hydrogen desorption traces shows that the first peak (β_1) corresponds to desorption of three hydrogen atoms per adsorbed cyclopentene molecule and indicates that dehydrogenation leads to a C_5H_5 species.[27] The line shape of the hydrogen evolution at higher temperature is similar to that observed for benzene on Pt(111),[2,30,31] which suggests that the adsorbed C_5H_5 species should be an aromatic cyclopentadienyl complex as already proposed by Avery.[27] The hydrogen desorption saturates at an exposure of 1.7 langmuir, and only then desorption of molecular cyclopentene can be observed. The TPD spectra of cyclopentene from Pt(111), which we present here, are in good agreement with previously reported results.[26−28] The good separation of the multilayer and the monolayer desorption peaks allowed us to easily prepare the saturation coverage in the monolayer by annealing a cyclopentene multilayer at 200 K. Since no ordered superstructures of the molecular layer have been found in LEED, it was not possible to estimate the absolute saturation coverage of the cyclopentene in the monolayer. Henn et al. estimated the saturation coverage of cyclopentene to 0.24 molecules per surface atom,[28] a result that we can neither confirm nor challenge at this point.

Figure 2 shows vibrational spectra of cyclopentene on Pt(111). The multilayer spectrum and the monolayer spectrum of cyclopentene on Pt(111) are in good agreement with measurements reported by Avery;[26,27] in our spectra, however, the resolution is much better. In the multilayer spectrum, the energetic positions of the peaks correspond quite well to those of the free molecule.[32] In particular, the prominent modes δCCC (75 meV) and ωCH (87 meV) are close to the gas-phase values of 74 and 86 meV, respectively.[32] Furthermore, the presence of the stretching mode of the olefinic hydrogen νCH at

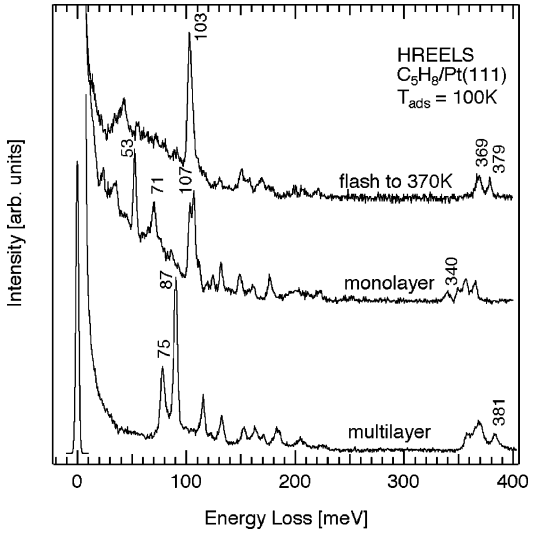

Figure 2. HREEL spectra of cyclopentene adsorbed on Pt(111). The monolayer was prepared by flashing the multilayer to 200 K.

381 meV points to an undisturbed double bond as is expected for a physisorbed molecule.

After flashing to 200 K, the spectrum denoted as "monolayer" is obtained. It corresponds to a saturation coverage of cyclopentene on Pt(111). The changes in the spectrum are easily visible. The absence of the olefinic νCH mode at 381 meV hints at a rehybridization of the olefinic carbon atoms and a di-σ bonding of the adsorbed molecule with the surfaces as has been previously reported by Avery.[26,27] A new loss peak appears at 341 meV, which has been assigned to a softened CH stretching mode, arising from hydrogen bonding to the substrate. The exact nature of this mode will be discussed below. The only other mode, which can be assigned rather safely, is the frustrated translation of the molecule against the surface νPtC_{sym} at 53 meV. All other modes are hard to assign on the basis of the symmetry of the undisturbed molecule since the chemisorption changes the nature of the molecule quite a bit. We will refer to this in the discussion.

Heating a monolayer of cyclopentene to 370 K yields a spectrum that is very similar to that of adsorbed benzene,[2] confirming the presence of an aromatic adsorbate that can be identified as cyclopentadienyl.[26,27] The spectrum is dominated by a loss at 103 meV belonging to the out of plane wagging mode ωCH. The CH stretching modes at 369 and 379 meV are shifted to higher energies implying higher C−C bond orders than in the case of cyclopentene.

The HREELS measurements are complemented and confirmed by the valence band photoemission spectra in Figure 3. The spectra show upon cyclopentene adsorption an initial damping of the Pt d-band region. This is accompanied by the emergence of a rather broad peak system in the range of 4−10 eV, which is related to the chemisorption of cyclopentene. After an exposure of 4 langmuir and above, a further dramatic change in the spectra takes place that results in a clear peak at 3.7 eV, a broad feature between 5 and 9 eV, and a second feature around 10.5 eV. These emissions can easily be related to the electronic states of physisorbed cyclopentene. The corresponding electronic states of the free molecule are also shown in the figure. To account for the work function and relaxation effects, their energetic position was chosen such that the 12a′ orbital corresponds to the peak at 3.7 eV and the relative positions of all other orbitals were kept constant. The spectra clearly show, as in the case of the HREELS results, that the chemisorbed

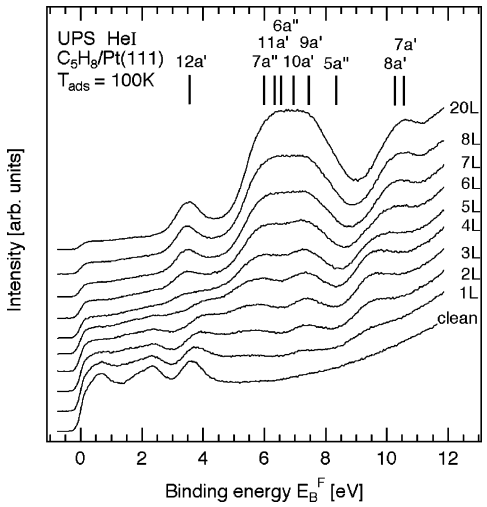

Figure 3. Evolution of the valence band photoemission for cyclopentene adsorbed on Pt(111) at 100 K as a function of exposure. The bars represent the gas-phase values for the designated orbitals (ref 32). These were adjusted such that the 12a′ orbital was used as a reference point.

species significantly differs from the physisorbed molecule, thereby again suggesting a di-σ bonding. A detailed analysis of the changes in the electronic structure of the molecule will be given together with the theoretical results in the discussion below. Saturating the surface with cyclopentene leads to a decrease of the work function of -1.55 eV in agreement with the value found by Avery.[27]

Adsorption of Cyclopentene on the Pt_3Sn/Pt(111) and Pt_2Sn/Pt(111) Surface Alloys. After the main features of the cyclopentene adsorption on Pt(111) have been discussed above, we now turn to the presentation of the results for the two surface alloys Pt_3Sn/Pt(111) and Pt_2Sn/Pt(111), respectively. On both surface alloys, large changes compared to the pure Pt(111) surface are visible in the TPD spectra (Figure 4). First of all, the desorption of molecular cyclopentene ($m/e = 67$) can be already detected for exposures as low as 0.2 langmuir on both surfaces. This fact is complemented by the absence of any trace of hydrogen desorption. These two results prove that both surface alloys are not active for dehydrogenation and that the cyclopentene adsorption is completely reversible. Furthermore, a significant decrease of the desorption temperatures of cyclopentene can be seen. On Pt_3Sn/Pt(111), small amounts of cyclopentene desorb at 260 K. This temperature can be translated into a desorption energy of 72 kJ mol^{-1} assuming a pre-exponential factor of 10^{13} s^{-1} in the framework of a first-order Redhead analysis. Accordingly the desorption temperature of 222 K on the Pt_2Sn/Pt(111) surface alloy yields a desorption energy of 61 kJ mol^{-1}. It can also be seen that in both cases a significant shift of the desorption maxima to lower temperatures for higher exposures takes place, suggesting a repulsive interaction between the adsorbed molecules. The desorption temperatures reported here are close to those found for ethene on Pt_3Sn/Pt(111) (240 K) and Pt_2Sn/Pt(111) (184 K),[10,11] suggesting that the bonding mechanism of ethene and cyclopentene on these surfaces is similar.

As has been stated above, the determination of the saturation coverage of the cyclopentene is not an easy task. However we attempted to get information about the relative amount of cyclopentene adsorbed on the two surface alloys compared to Pt(111). A careful analysis of the TPD peak areas in the spectra from the three surfaces points to the fact that equal amounts of cyclopentene can be adsorbed on each of them. We will come back to this point later in the discussion.

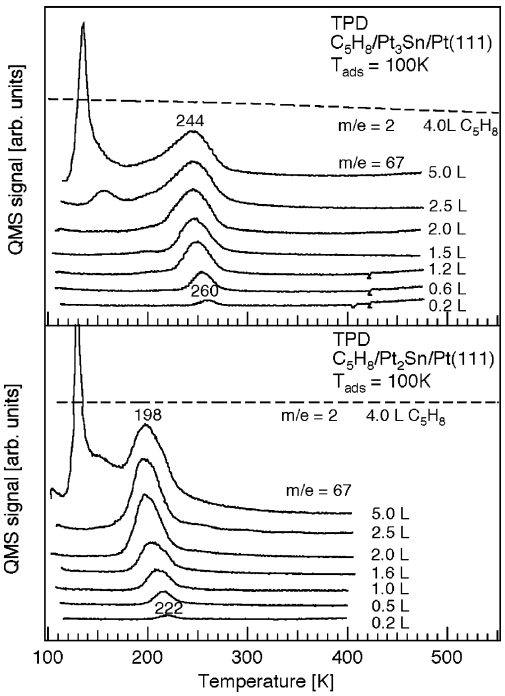

Figure 4. TPD spectra of cyclopentene absorbed on Pt_3Sn/Pt(111) (top) and Pt_2Sn/Pt(111) (bottom) at 100 K. The dashed line in both graphs represents the desorption trace of reactively formed hydrogen ($m/e = 2$) on the respective surface. The heating rate was 2 K s^{-1} for all spectra.

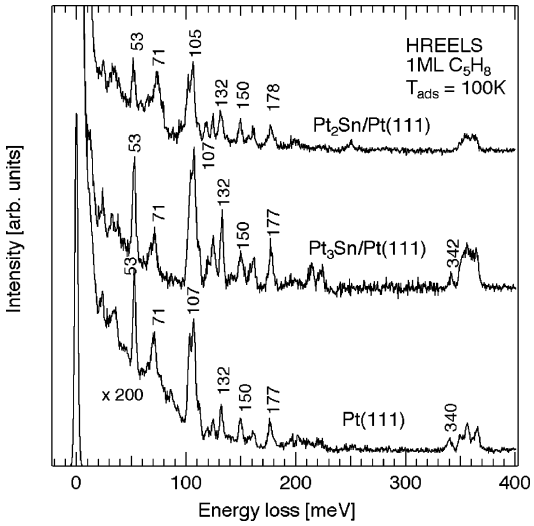

Figure 5. Comparison of the HREEL spectra of a full monolayer of cyclopentene adsorbed on Pt(111), Pt_3Sn/Pt(111), and Pt_2Sn/Pt(111) at 100 K.

Considering the weaker bonding of the molecule on the surface alloys, the question arises whether the bond type of the cyclopentene is also changed on these surfaces. A first indication can be derived from the HREEL spectra that are displayed in Figure 5. Here monolayer coverages of cyclopentene on the three surfaces in question are compared. Already a first visual inspection shows that the main features in the spectra on both Pt_nSn/Pt(111) surface alloys are very similar to those of cyclopentene on the pure Pt(111) surface. Again the di-σ bonding of the molecules can, therefore, be inferred. However, there is a marked difference between the Pt_3Sn/Pt(111) and the Pt_2Sn/Pt(111) surface. On the former, the νCH soft mode is detectable at 342 meV, whereas this is not the case for the latter. This observation clearly indicates that there is no agostic (Pt$\cdots$H$-$C) bonding on the Pt_2Sn/Pt(111) surface alloy as on

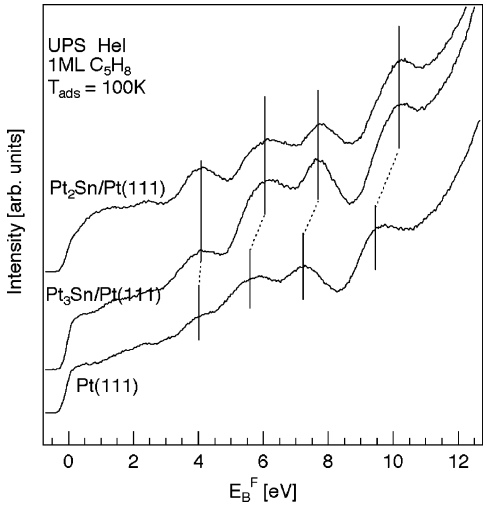

Figure 6. Comparison of the UP spectra of a full monolayer of cyclopentene adsorbed on Pt(111), Pt_3Sn/Pt(111), and Pt_2Sn/Pt(111) at 100 K.

the two other surfaces. Most surprisingly, the molecule surface vibration νPtC_{sym} (~53 meV) remains virtually unchanged on the surface alloys even though the corresponding bond is much weaker.

In Figure 6, the HeI UP spectra of a monolayer of cyclopentene on Pt(111) and the Pt_nSn/Pt(111) surface alloys are displayed. It can be seen that the structure of the valence band is very similar in all cases. All spectra can be characterized by four peaks in the range from 3.5 to 11 eV. There are slight differences in the peak shapes and the energetic positions of the peaks. However the result obtained from HREELS that the bonding on all three surfaces is of the same type (di-σ) can also be confirmed on the basis of the UPS results. Due to the complex electronic structure of the cyclopentene, we have not attempted to fit the peaks to certain electronic states but rather leave the task of interpreting the spectra to the detailed discussion below.

In the case of the two surface alloys, UPS measurements gave a work function decrease of −1.3 eV for a saturation coverage of cyclopentene.

Discussion

Cyclopentene on Pt(111). The presentation of the experimental data above leaves some open questions that call for a theoretical treatment of the system in order to gain a detailed understanding of the adsorption modes and geometries of the cyclopentene. To accomplish this, we performed density functional calculations for cyclopentene adsorption. For the adsorption on Pt(111), three different unit cells were used, which are displayed in Figure 7. The first one contains 9 atoms per layer, giving a 3 × 3 structure and a cyclopentene coverage of 1/9 ML (Figure 7a showing the di-σ configuration). A unit cell containing 7 atoms per layer was also considered. A ($\sqrt{7} \times \sqrt{7}$)R19° structure is obtained with a coverage of 1/7 ML (Figure 7b with the di-σ configuration), which corresponds to the structure assumed for the maximum coverage of cyclopentadienyl, product of the decomposition of cyclopentene.[27] Since the saturation coverage of cyclopentene on Pt(111) has been estimated to be 0.24 ML,[28] a unit cell containing 4 metal atoms per layer was finally simulated. This unit cell leads to a 2 × 2 structure and a coverage of 1/4 ML, which is illustrated for the di-σ configuration (Figure 7c) as well as for two different π configurations (Figure 7d,e). The Brillouin zone integration has been done on a 3 × 3 × 1 grid for a coverage of 1/9 ML and on a 5 × 5 × 1 grid for coverages of 1/7 ML and 1/4 ML.

After adsorption, the molecule, which is planar in the gas phase, looks like cyclopentane and bends as shown in Figure 8. The middle methylene group C^4H_2 can be directed either toward the surface (**A**) or in the opposite direction (**B**). Conformation **B** has been calculated for the di-σ geometry at coverages of 1/4 ML and 1/9 ML. It is less stable than **A** by 6 and 8 kJ mol^{-1}, respectively. In **B**, the molecule must probably bend too much in order to avoid steric repulsions of the hydrogen atoms with the surface (angle ω is 140° compared with 147° as noted in Table 2). Hence conformation **A** is the most stable one and will be considered further. This result is in contradiction to the assumption of Avery[27] and Brizuela et al.,[33] who both predicted the adsorbed cyclopentene to be planar.

In the di-σ geometry, the double bond interacts with two platinum atoms and the median carbon C^4 lies above a platinum atom. In the π geometry, the double bond interacts with only one surface atom. Two situations exist: either C^4 lies between two Pt atoms (Figure 7d) or it lies above one Pt atom (Figure 7e). The latter case is energetically more favorable by 4−6 kJ mol^{-1} and will be considered hereafter. The adsorption energies are given in Table 1. For all coverages, the π adsorption is less stable than the di-σ one by 26−30 kJ mol^{-1}, which confirms the experimental finding that cyclopentene adsorbs in the di-σ geometry on Pt(111). The values of the adsorption energies at coverages of 1/7 ML (93 kJ mol^{-1}) or 1/9 ML (94 kJ mol^{-1}) are in accord with the experimental value of the desorption energy (79 kJ mol^{-1}, desorption peak at 286 K). However, the energy strongly decreases to 49 kJ mol^{-1} for a coverage of 1/4 ML. This value is much lower than the experimental finding. The work function decrease after adsorption is also reported in Table 1. It increases with the coverage reaching −1.5 eV for the di-σ geometry at 1/7 ML and −2.0 eV at 1/4 ML. The former value is in good agreement with the value of −1.55 eV, which has been deduced from UPS. The negative value of $\Delta\Phi$ reflects that the π donation prevails over the back-donation in the interaction.

A detailed overview of main bond lengths is given in Table 2 (for atom numbering see Figure 8). In the di-σ mode, the C^1-C^2 bond length is strongly elongated from its value in the gas phase (1.336 Å) and has the character of a single bond, which reflects the strong interaction. The lengthening is weaker for the π mode, which shows, in addition to the longer Pt−C bond, that this mode is less stable. For the di-σ geometry at 1/7 and 1/9 ML, the distance Pt^3-H_β is relatively short (2.35, 2.38 Å) and the C^4-H_β bond is long (1.113−1.115 Å) compared with the other methylene groups (1.098 Å). This situation corresponds to short Pt^1-C^1 and Pt^2-C^2 bonds and to the smallest values of the bending angle ω of the cyclopentene cycle (angle between the planes $C^1C^2C^3$ and $C^3C^4C^5$) and of angle α between the plane $C^1C^2Pt^1Pt^2$ and the vertical. These values suggest the formation of a Pt^3-H_β bond, which has been inferred from the appearance of the soft mode in HREELS. This result again contradicts the findings of Avery[27] who postulated that the soft mode is due to either the olefinic $C^{1,2}H$-groups or the $C^{3,5}H_2$-groups.[27] At 1/4 ML, ω is greater and the Pt^3-H_β distance is longer because of steric effects. For the π geometries also at coverages of 1/7 and 1/9 ML, the Pt^3H_β distance is relatively small, though longer than for the di-σ geometries. Again at 1/4 ML, this distance is long. Angle ω is smaller but α is greater, which means that there is a compromise between correct angles in the cycle and the release of steric effects.

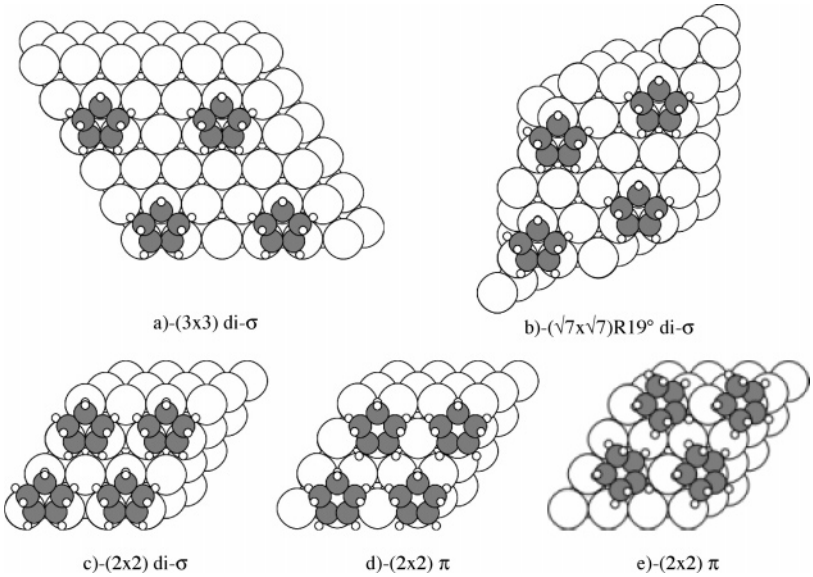

Figure 7. Representation of the di-σ and π adsorption geometries of cyclopentene on Pt(111) used in the DFT calculations for various coverages: (a) 1/9 ML; (b) 1/7 ML; (c−e) 1/4 ML.

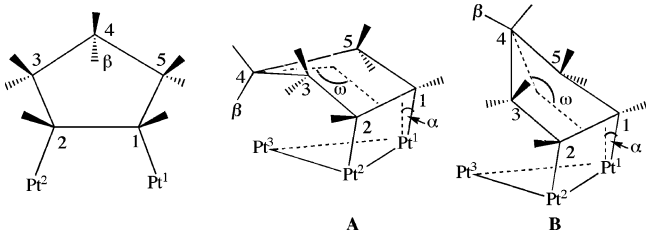

Figure 8. Schematic representation of the adsorbed cyclopentene molecule and two different conformers.

TABLE 1: Adsorption Energies E_{ads} (in kJ mol^{-1}) and Work Function Changes $\Delta\Phi$ (in eV) of Cyclopentene on Pt(111) for the Different Adsorption Geometries and Coverages

		theory at the following coverages [ML]			experiment, saturation
		1/4	1/7	1/9	
di-σ	E_{ads}	49	93	94	79
	$\Delta\Phi$	−2.0	−1.5	−1.3	−1.55
π	E_{ads}	22	63	68	
	$\Delta\Phi$	−2.3	−1.8	−1.6	

TABLE 2: Main Bond Lengths (in Å), Bending Angle ω, and Angle α with the Vertical (in Degrees) for the di-σ and π Adsorption Geometries of Cyclopentene on Pt(111) at Various Coverages[a]

	di-σ at the following coverages [ML]			π at the following coverages [ML]		
	1/4	1/7	1/9	1/4	1/7	1/9
Pt−C^1	2.130	2.131	2.137	2.216	2.220	2.234
C^1−C^2	1.497	1.504	1.504	1.412	1.418	1.416
C^2−C^3	1.528	1.532	1.531	1.512	1.513	1.512
C^3−C^4	1.520	1.532	1.531	1.534	1.539	1.539
Pt−H$_\beta$	2.604	2.380	2.346	2.786	2.428	2.388
C^4−H$_\beta$	1.107	1.113	1.115	1.103	1.110	1.112
ω	150	147	147	148	154	154
α	5	4	4	14	7	7

[a] The atom numbering follows Figure 8.

The results presented above clearly favor the di-σ geometry over the π geometry. To verify this, the HREEL spectra for the different geometries were calculated (Figure 9). Already a first visual comparison with the experimental HREEL spectra in Figure 2 shows that the di-σ geometry closely corresponds to the experimental data. In particular, the prominent peaks at 48 meV (νPtC$_{sym}$) and 107 meV (νC^{1}C^2 + γCH$_{sym}$(C^{1}C^2)) are present in the calculated spectra of the di-σ geometry but absent in those of the π geometry, as well as the soft νCH mode at 345 meV. This again justifies the notion of a di-σ bonding. Furthermore, the detailed assignment of the most important vibration modes given in Table 3 shows that the energies do not vary much with the coverage and are in excellent agreement with the experimental values.

One particular difference concerns the so-called soft mode. According to our results, this mode is a consequence of the Pt^3−H$_\beta$ bond, which softens in turn the corresponding ν(CH$_\beta$) vibration. When the coverage increases, this soft νCH mode disappears: it still exists for 1/7 ML, although the gap with the other νCH modes is smaller, but joins them for 1/4 ML. This shift is also visible in the experimental results. Figure 10 shows the CH-stretch region of the HREEL spectra for two different exposures. The spectra were fitted with four Gaussians of 3 meV full width at half-maximum (fwhm), which was the experimental resolution in both cases, and the position of the modes was hence extracted. As for the calculated values, the ν(CH$_\beta$) mode is at smaller energy for smaller exposure (336 vs 340 meV). This validates the shift of the peak position, which was observed theoretically.

To further investigate the interaction between the cyclopentene and Pt(111) surface, the density of states (DOS), which was projected on the interacting orbitals d_{z^2} and d_{xz} for Pt^1 (Pt^2) as well as p_z for C^1 (C^2) (Figure 11), has been plotted in Figure 12. We have also plotted the DOS projected on the H$_\beta$ s orbital (Figure 12f) and the d_{z^2} orbital of Pt^3 (Figure 12h). The DOS projected on the d_{z^2} and d_{xz} orbitals of a noninteracting platinum atom is shown for comparison (Figure 12a,b). The DOS projected on the p_z orbital of C^1 for a noninteracting cyclopentene in the adsorbed geometry is also plotted (Figure 11g).

In the DOS projected on d_{z^2} Pt^1 or d_{xz} Pt^1, one clearly observes peaks at −14.5, −14.0, −12.4, and −11 eV as well as in the range from −5 to 0.5 eV, which are derived from the hybridization of the platinum and the cyclopentene orbitals. The peaks at −14.5, −12.4, and −11 eV correspond to the C^1 p_z orbital (Figure 12e). The peak at −14 eV corresponds to the C^1 p_x (not shown in the figure). In fact, owing to the hybridization of the carbons C^1 (and C^2), the p_z and p_x orbitals

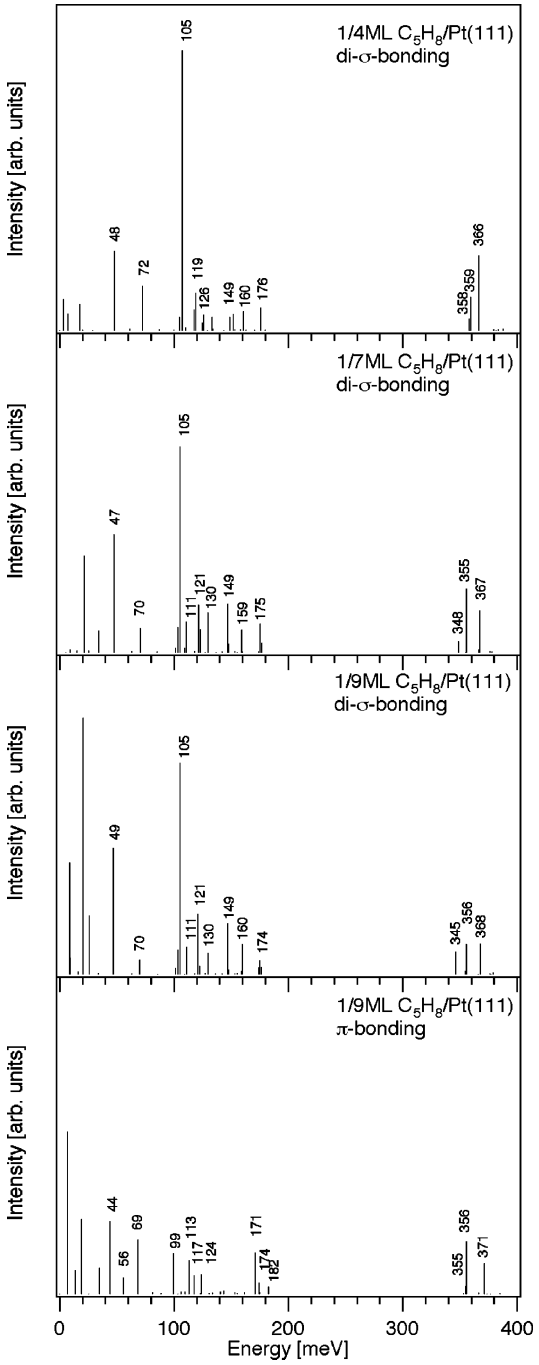

Figure 9. Calculated HREEL spectra for cyclopentene adsorbed on Pt(111) in the di-σ geometry at coverages of 1/4, 1/7, and 1/9 ML and in the π geometry at a coverage of 1/9 ML.

mix to give hybridized π and π^* orbitals, which explains the participation of the C^1 p_x orbital in the interaction (see Figure 11). The unoccupied part of the DOS projected on p_zC^1 is divided in two parts, one between -5 and 0.5 eV and the other between 0.5 and 6 eV. The former corresponds to the π^* orbital, and the latter rather to σ^*_{CC} or σ^*_{CH} orbitals. This assignment is derived from the comparison of the DOS projected on the orbitals of the other carbons C^3 and C^4 not shown here. Compared to the d_{z^2} orbital of a noninteracting platinum (Figure 12a), the Pt^1 d_{z^2} orbital is pushed away from the Fermi level E_F toward lower energies and has a large contribution above this level. There are two possible reasons. The first one is the four-electron interaction of Pauli type between the occupied π orbitals and the almost full d-band of platinum, which stabilizes the π orbital and destabilizes the d-band. The peaks at -14, -12.5, and -11 eV, corresponding to the π system of cyclopentene, reflect this interaction. The crossing of part of the d-band above E_F results in a stabilizing interaction. The second reason is the back-donation from the d-band to the π^* orbitals of cyclopentene, the antibonding combination of which appears above E_F. Hence, the large band between -5 and 0.5 eV corresponds to interactions of d_{z^2} with both π and π^*. The DOS projected on d_{xz} (Figure 10d) does not show peaks above E_F but only peaks at -14.5 and -11 eV corresponding to the π system of cyclopentene. In this case, no shift of the d-band above E_F is observed. Effectively, following Figure 11, the π^* orbital can interact with the antibonding combination of the d_{z^2} or the d_{xz} orbitals of Pt^1 and Pt^2, which lies at the top of the d-band. For d_{z^2}, the overlap is maximal. By contrast, π^* overlaps with both the positive and the negative parts of d_{xz}, which reduces considerably the total overlap. Hence the interaction of π^* with d_{xz} is small.

The DOS projected on d_{z^2} Pt^3 shows some differences compared to the noninteracting Pt atom (Figure 12h,a); particularly the peak just below E_F is higher. Moreover, the small peak at -14.5 eV corresponds to the s orbital of H_β (Figure 10f), which reflects the formation of a weak bond between H_β and the surface.

To be able to compare these results with the experimental UP spectrum, the DOS projected on all atoms of the molecule has been calculated and displayed in Figure 13. Four bands are observed, which are centered around 3.9, 5.4, 7.3, and 9.1 eV. These states compare quite well to the experimental spectrum, which is also given in Figure 13 and possesses peaks at 4, 5.5, 7.2, and 9.5 eV. It is difficult to assign the peaks to particular molecular orbitals because they all mix together owing to the loss of flatness. The calculation of the cyclopentene molecule in the di-σ adsorption geometry shows that orbitals of the free molecule 9a′ and 10a′ on one hand and orbitals 7a′ and 8a′ on the other hand (see Figure 14) mix to give a high-lying antibonding and a low-lying bonding combination. The order of the orbitals is now 12a′, 10a′$-$9a′, 7a″, 11a′, 6a″, 9a′$+$10a′, 5a″, 8a′$-$7a′ and 8a′$+$7a′. After adsorption, the orbitals are even more perturbed. For instance, the p_zC^1 orbital representing the π molecular orbital does not appear as a single peak but as several peaks and bands distributed below the Fermi level (Figure 12e). The easiest orbitals to recognize are 7a″, 11a′, 10a′, and 9a′. 7a″ is a combination of p_xC^4 and p_xC^3 or p_xC^5 and corresponds to the first peak below E_F at -3.7 eV. 11a′ is a combination of p_yC^4 and p_yC^3 or p_yC^5 and appears at -4.1 eV. 9a′ and 10a′ give two combinations mainly centered on p_zC^4 and p_xC^1 and positioned at -7.6 eV and around -4 eV. At -7.6 eV is also found 6a″ which is a combination of p_yC^1 and p_yC^2. The last two peaks at -8.9 and 9.5 eV are mixtures of several molecular orbitals and cannot be attributed precisely. The π orbital is distributed between peaks at -4.1 eV (under 7a″), -5.8 eV (as a shoulder of the large peak centered at -5.4 eV), -7 eV, and -9.5 eV.

Cyclopentene on the Pt_nSn/Pt(111) Surface Alloys. Because we have already identified the di-σ adsorption mode to be more stable than the π bonding on the pure Pt(111), we have restricted our analysis of the adsorption on the surface alloys to this configuration. This is also in line with the results of Paffett et al., who had already shown that ethylene keeps the di-σ adsorption geometry on the $Pt_nSn(111)$ surface alloys.[3] Again several different unit cells have been used to model the adsorption system. For the Pt_3Sn/Pt(111) surface alloy, two unit cells were considered. The first contains 8 atoms per layer and

TABLE 3: Positions (in meV) and Assignments of the Calculated HREELS Peaks Together with the Corresponding Experimental Values for the di-σ Geometry of Cyclopentene on Pt(111), Pt_3Sn/Pt(111), and Pt_2Sn/Pt(111)

	Pt(111)				Pt_3Sn(I)(111)		Pt_2Sn(111)	
	theory at the following coverages [ML]			experiment, saturation	theory at 1/12 ML coverage	experiment, saturation	theory at 1/9 ML coverage	experiment, saturation
	1/4	1/7	1/9					
νPtC_{sym}	48	47	49	53	48	53	47	52
δCCC	72	70	70	71	65	71	72	74
$\nu C^1C^2 + \gamma CH_{sym}(C^1C^2)$	107	105	105	107	104	107	106	105
νCC_{sym} (C^2C^3, C^1C^5) + γCH		111	111	112	110	112	111	112
ρCH_2 (C^4)	119	121	121	119	122	119	124	118
ρCH_{2sym} (C^3, C^5) + γCH_{sym}	126	130	130	132	130	132	130	132
νCC_{sym} (C^2C^3, C^1C^5) + νC^1C^2	149	147	147	150	147	150	149	150
$\omega CH_{2\,sym}$ (C^3)	160	159	160	159	160	161	155	161
δCH_2 (C^4) + δCH_2 (C^3, C^5)	176	175	174	177	176	177	176	178
νCH_β	358	349	345	340	352	342	361	
νCH (C^3, C^5)	359	355	356	356	356	357	356	356
νCH (C^3, C^5)	366	367	368	365	366	364	367	363

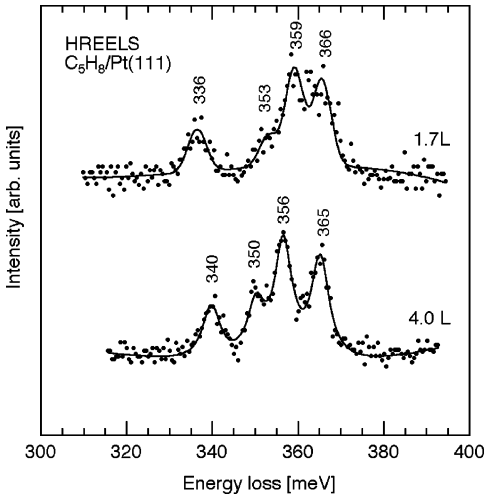

Figure 10. Experimental HREEL spectra (dots) for two different exposures of cyclopentene adsorbed on Pt(111). Only the νCH region is shown. The solid lines represent the best fit to the spectra using Gaussian functions with a fwhm of 3 meV, which corresponds to the experimental resolution. The indicated peak positions are taken from the fits.

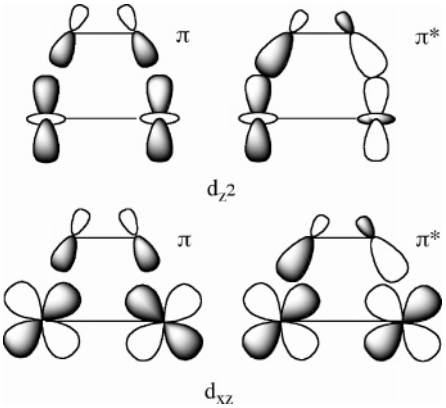

Figure 11. Schematic interactions between the d orbitals of the Pt surface atoms and the π-system of cyclopentene in the di-σ geometry.

results in a 4 × 2 structure with a coverage of 1/8 ML. In this case, two different positions of H_β, above a Pt atom (Figure 15a, **I**) and above a Sn atom (Figure 15b, **II**), are possible. The second unit cell contains 12 atoms per layer, which yields a $2\sqrt{3} \times 2\sqrt{3}$ structure with a coverage of 1/12 ML (Figure 15c). Again the two different configurations are possible, only one of which is shown here. In the case of the Pt_2Sn/Pt(111) surface alloy, only a coverage of 1/9 ML has been used (Figure 15d). In this case, H_β is always located over a Sn atom. The Brillouin zone integration has been done on a 3 × 3 × 1 grid for coverages of 1/9 and 1/12 ML and on a 5 × 3 × 1 for a coverage of 1/8 ML. For this alloy, conformation **B** (Figure 8) has also been tested. Despite the presence of the Sn atom, the methylene C^4H_2 group prefers to be oriented toward the surface as in **A**. Conformation **B** is less stable than **A** by 6 kJ mol^{-1}.

The adsorption energies are given in Table 4. In the case of Pt_3Sn, the two geometries have almost the same energy, **I** being more stable by 3 kJ mol^{-1}. Therefore, the two structures should coexist on the surface. A large decrease of the adsorption energy on Pt_3Sn/Pt(111) compared to Pt(111) is observed (42 vs 94 kJ mol^{-1}). This trend is even more pronounced for Pt_2Sn/Pt(111) where the adsorption energy is only 30 kJ mol^{-1}. This corroborates the decrease observed experimentally (79, 72, and 61 kJ mol^{-1}) although the difference between platinum and the alloys is greater in the calculations. One reason for this could be that on the Pt(111) surface there is a competition between desorption and dehydrogenation, which in general leads to an underestimation of the desorption energy at low coverage.

The geometry optimization of the adsorbate yields a result that is quite similar to that obtained for Pt(111) with a slightly longer cyclopentene−surface bond (PtC^1 bond) (Table 4). When H_β is located above a Sn atom (Pt_3Sn(II) and Pt_2Sn), the distance of H_β to the surface (Sn−H_β) is long (more than 2.6 Å). In the case of Pt_3Sn(I), the Pt−H_β distance is relatively short (2.48 Å) although it is longer than in the case of the adsorption on Pt(111) at coverages of 1/7 and 1/9 ML, either in the di-σ or in the π geometry. The angles ω and α are greater for the geometries where H_β is above a Sn atom in order to release the repulsive interaction with this surface atom.

The calculated HREEL spectra for the di-σ adsorption geometry on Pt_3Sn(I) and Pt_3Sn(II) at 1/12 ML and on Pt_2Sn are shown in Figure 16. The spectra compare well with the experimental ones shown in Figure 4. The energetic positions of the most important loss peaks are given in Table 3. Except for νCH vibrations, they do not differ much from those of cyclopentene on Pt(111) at coverages of 1/7 and 1/9 ML, respectively. One finds again the high peaks around 48 meV (νPtC_{sym}) and 105 meV ($\nu C^1C^2 + \gamma CH_{sym}(C^1C^2)$). There are more peaks between 105 and 180 meV than in the spectrum calculated for the di-σ geometry on Pt(111) at 1/9 ML, and those peaks are more intense in the case of Pt_3Sn(I). This is also observed experimentally. In the calculated spectrum for Pt_2Sn, two peaks at 72 and 100 meV have a much higher intensity than in the case of Pt. Both peaks correspond to a bending mode of the C^4H_2 group along the vertical. This motion is wider when C^4 and H_β are farther from the surface, and the variation of the

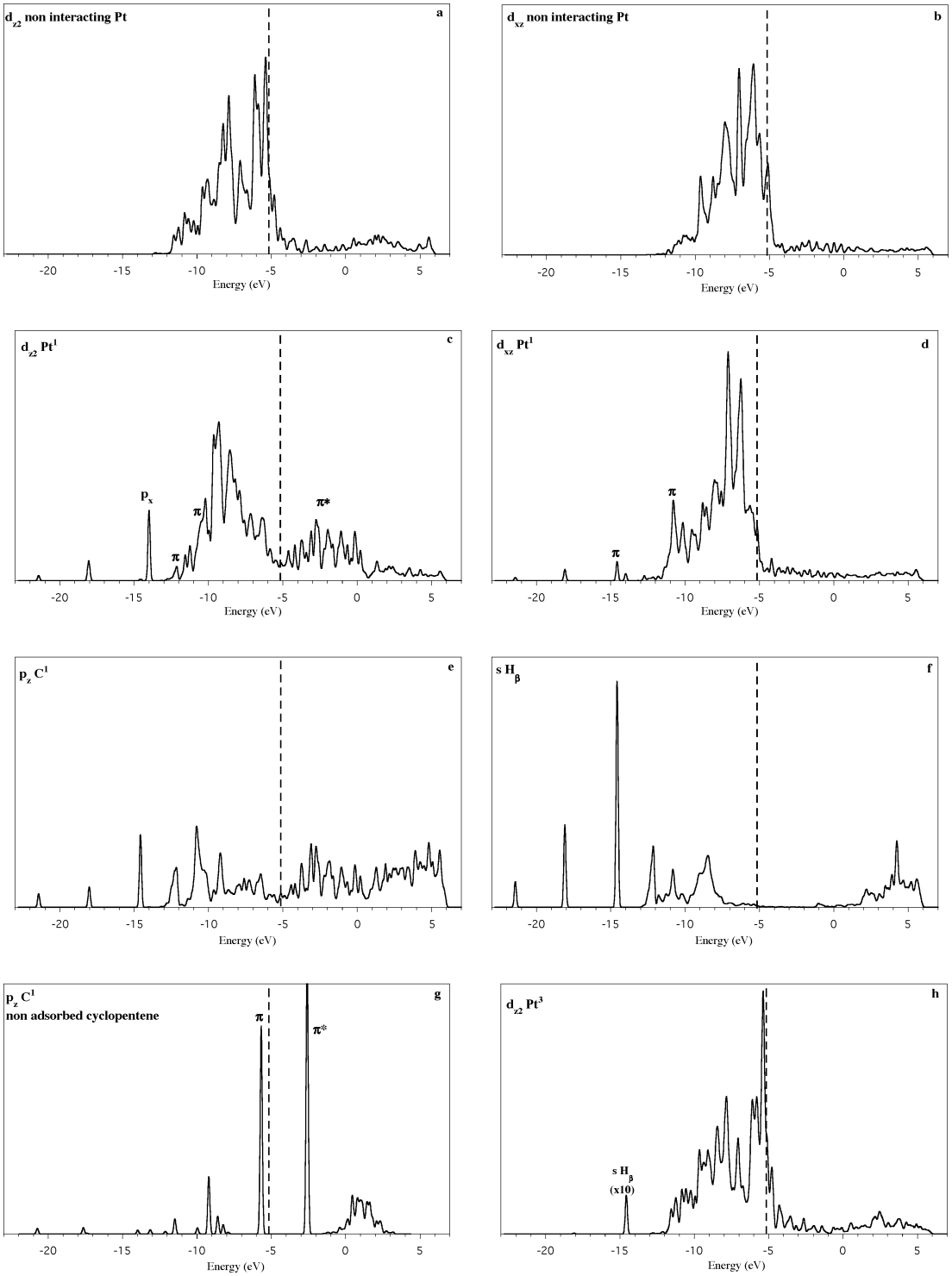

Figure 12. Projected DOS for the di-σ adsorption of cyclopentene on Pt(111): (a,b) d_{z^2} and d_{xz} orbitals of a noninteracting Pt surface atom; (c,d) d_{z^2} and d_{xz} orbitals of an interacting Pt surface atom (Pt^1). Projected DOS of the p_z orbital of the interacting carbon atom C^1: (e) when adsorbed; (g) in the gas phase but with the geometry as adsorbed. Projected DOS of (f) the s orbital of H_β, and (h) the d_{z^2} orbital of Pt^3. The dashed line marks the position of the Fermi energy. The atom numbering is given in Figure 8.

dipole is larger, which results in an increased intensity of the peaks. The presence of Sn also can play an electrostatic role in the variation of the dipole. Concerning the νCH stretching modes, a small peak corresponding to the C−H_β vibration exists in the case of Pt_3Sn(I), at a higher frequency than on Pt(111): 352 vs 345 meV. This means that a weak interaction exists between H_β and the surface for this low coverage, signified by a short Pt^3−H_β distance and a long C^4H_β bond (2.482 and 1.111 Å, respectively; Table 4). The other νCH stretches are more intense than in the other spectra, in agreement with the experimental results. At 1/8 ML, the νCH_β vibration is still higher in energy and less intense (spectrum not given here), which shows that when the coverage increases, the interaction of H_β with the surface becomes weaker, as it does also on Pt. The soft stretch does not exist in the case of Pt_2Sn: the νCH_β vibration appears at 361 meV and is not the lowest one (Table 4). This is in relation with the long distance between H_β and the surface due to the presence of the Sn atom. In the

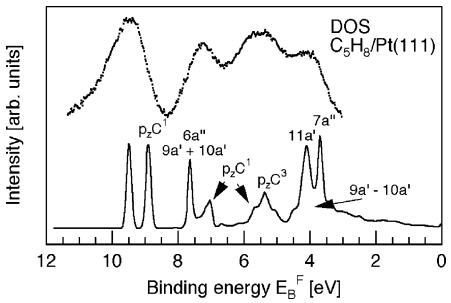

Figure 13. DOS projected on all carbon and hydrogen atoms of cyclopentene adsorbed in the di-σ geometry on Pt(111) (line) and the corresponding UP spectrum (dots). The UP spectrum is the difference between the spectrum of the clean Pt(111) surface and that of a full monolayer coverage of cyclopentene on this surface.

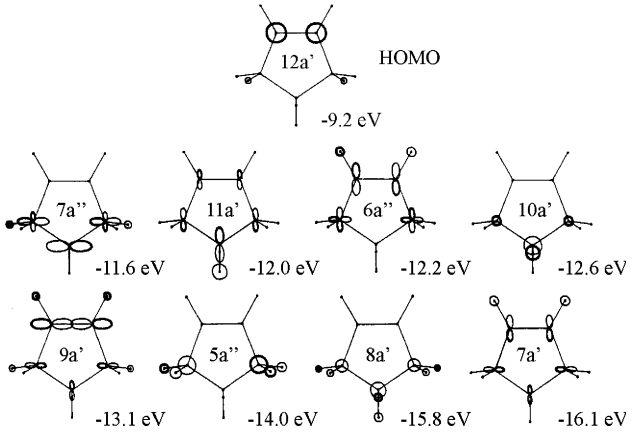

Figure 14. Molecular orbitals of the free cyclopentene molecule (from ref 34).

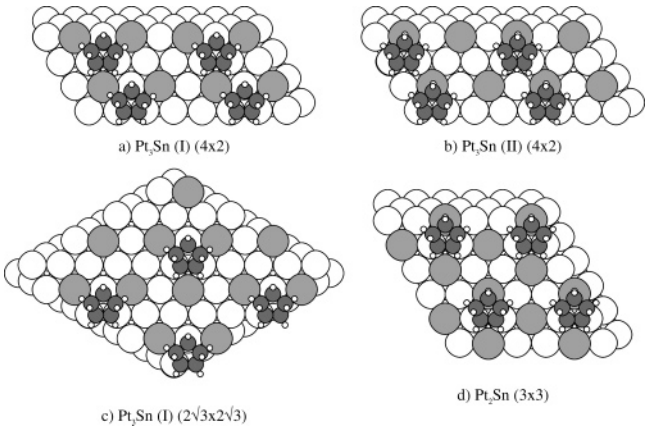

Figure 15. Schematic representation of the di-σ adsorption geometry I of cyclopentene on Pt_3Sn at coverages of 1/8 and 1/12 ML and geometry II at a coverage of 1/8 ML as well as on Pt_2Sn at a coverage of 1/9 ML.

experimental spectrum also, no soft stretch is observed. Hence the calculated spectra reproduce well the experimental ones, confirming that cyclopentene is adsorbed in the di-σ geometry on the Pt−Sn alloys.

We have already studied the electronic structure of the Pt_3-Sn and Pt_2Sn alloys compared to that of Pt and the modifications of the DOS shape of a surface platinum atom when Sn is present.[6] The surface platinum atoms are more negatively charged in the case of the alloys, and their DOS is narrower and displaced from the Fermi level toward lower energies (see Figure 17a,b). The d-band gains the main part of the electron transfer from the Sn atoms and its center is lower relative to

TABLE 4: Adsorption Energies E_{ads} (in kJ mol^{-1}), Main Bond Lengths (in Å), Bending Angle ω, and Angle α with the Vertical (in Degrees) for the di-σ Adsorption Geometry of Cyclopentene on Pt_3Sn/Pt(111) and Pt_2Sn/Pt(111)[a]

	Pt_3Sn(I) at the following coverages (ML)		Pt_3Sn(II) at the following coverages (ML)		Pt_2Sn at 1/9 ML coverage
	1/8	1/12	1/8	1/12	
E_{ads}	42	46	39	43	30
Pt−C^1	2.145	2.144	2.148	2.147	2.138
C^1−C^2	1.497	1.507	1.486	1.501	1.504
C^2−C^3	1.534	1.534	1.534	1.534	1.536
C^3−C^4	1.532	1.530	1.537	1.535	1.535
Pt−H_β or Sn−H_β	2.502	2.482	2.659	2.624	2.673
C^4−H_β	1.110	1.111	1.105	1.105	1.105
ω	145	144	151	151	150
α	3	3	5	5	4

[a] The atom numbering follows Figure 8.

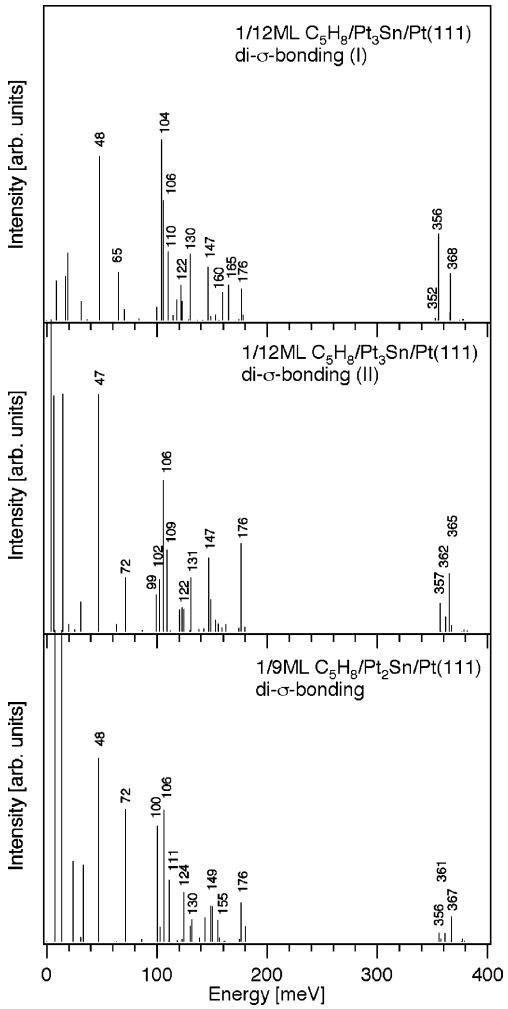

Figure 16. Calculated HREEL spectra for cyclopentene adsorbed in the di-σ geometries I and II on Pt_3Sn at a coverage of 1/12 ML and on Pt_2Sn at a coverage of 1/9 ML.

the corresponding Fermi level. Only the case of Pt_2Sn is studied in the following.

The DOS projected on the d_{z^2} and d_{xz} orbitals of the interacting platinum atoms is very similar to that obtained for pure platinum (Figure 17c,d). The same peaks corresponding to the p_z and p_x orbitals of C^1 are present. If the DOS projected on p_z C^1 in the case of Pt_2Sn and that in the case of Pt are compared, a small displacement of the peaks is observed toward the lower energies in the case of the alloy, particularly the peak at −10.5 eV

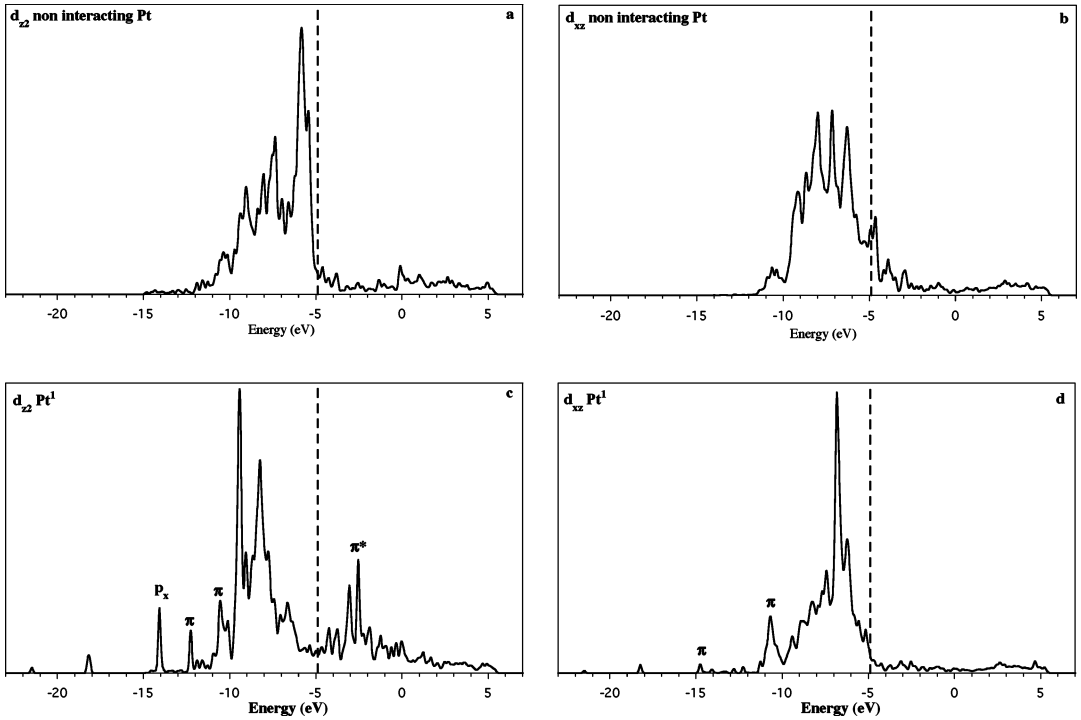

Figure 17. Projected DOS for the di-σ adsorption of cyclopentene on Pt_2Sn/Pt(111): (a,b) d_{z^2} and d_{xz} orbitals of a noninteracting Pt surface atom and (c,d) of an interacting Pt surface atom (Pt^1). The dashed line marks the position of the Fermi energy. The atom numbering is given in Figure 8.

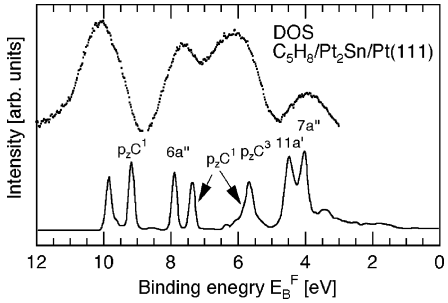

Figure 18. DOS projected on all carbon and hydrogen atoms of cyclopentene adsorbed in the di-σ geometry on Pt_2Sn/Pt(111) and the corresponding UP spectrum (dots). The UP spectrum is the difference between the spectrum of the clean Pt_2Sn/Pt(111) surface and that of a full monolayer coverage of cyclopentene on this surface.

(Figures 10c and 14c). Hence it seems that the interaction between the occupied π orbital and the metal d-band is slightly stronger in the case of Pt_2Sn, since the π orbital is more stabilized. This gives a more stabilizing or a less stabilizing interaction depending on the part of the d-band pushed above E_F. A displacement of the π^* orbital toward the lower energies is more easily observed: the band which is between E_F and 0.5 eV for Pt extends only to 0 eV for Pt_2Sn. This means that the back-donation into π^* is weaker for the alloy. Moreover, the d-band of the surface platinum atoms being more populated, the repulsive four-electron interactions with the occupied orbitals of cyclopentene are stronger. These arguments explain the weaker adsorption on the alloys.

For Pt_2Sn, the UP spectrum has been simulated and is displayed in Figure 18 together with the experimental spectrum. Both spectra are very similar to those obtained for cyclopentene on Pt(111) (Figure 13). Again four bands are observed with nevertheless different intensities. The molecular orbitals are more mixed, but 7a″, 6a″, and 11a′ can be attributed. Relative to the respective Fermi level (at 0 eV), the bands are lower in energy in the case of the alloy. For instance, 7a″ lies at 4 eV and 11a′ at 4.5 eV instead of 3.7 and 4.1 eV and the two last peaks appear at 9.2 and 9.9 eV instead of 8.9 and 9.5 eV. Even if the two Fermi levels are put at their actual values (−5.09 eV for Pt and −4.89 eV for Pt_2Sn), which is equivalent to shifting the DOS of the alloy by 0.2 eV toward higher energies, the bands remain lower in the case of the alloy. This confirms more obviously what was said just before about the position of the π orbital in the case of the alloy compared with Pt. Experimentally also, the four bands of the UP spectrum are displaced in the same direction in the case of the two alloys, compared with platinum (Figure 13). Hence the calculated spectra are in good agreement with the experimental ones.

We now come back to the question of whether the reduced adsorption energies of cyclopentene can be explained by a ligand or rather an ensemble effect. From the afore said and the comparison of the geometries (Tables 2 and 4) of the adsorbate on the three surfaces, it is obvious that the main difference is produced by the difference in the electronic structure of the Pt(111) and the two Pt_nSn/Pt(111) surface alloys, thus, a *ligand effect*. This view is also supported by the fact that the energetic difference between the two different configurations Pt_3Sn(I) and Pt_3Sn(II), a case where an ensemble effect is clearly expected, is only small.

Finally we discuss the issue of the absence of dehydrogenation on the two surface alloys. Two effects can play a crucial role. First, at low coverage on Pt(111) (1/7 and 1/9 ML) the distance Pt_3-H_β is small (2.380 and 2.346 Å, Table 2), whereas this distance is much larger on both alloys (Table 4). This already explains why the activation energy for the abstraction of H_β should be greater on the surface alloys. Second, we have shown previously that for benzene on Pt_nSn/Pt(111) no chemisorbed species exists. Given the close resemblance of cyclopentadienyl (C_5H_5) (the dehydrogenation product of cyclopentene on Pt(111)) to benzene on Pt(111), a possible reason for the absence of dehydrogenation can also be the lack of an appropriate adsorption site for the cyclopentadienyl.

Conclusions

The adsorption of cyclopentene on Pt(111) and on the ordered Pt_3Sn/Pt(111) and Pt_2Sn/Pt(111) surface alloys was investigated experimentally by TPD, UPS, and HREELS as well as theoretically by ab initio DFT calculations.

On Pt(111) and both Pt_nSn/Pt(111) surface alloys, cyclopentene is di-σ-bonded occupying bridge sites. A detailed analysis of the adsorption geometry based on the DFT calculation has been presented. It shows in the case of cyclopentene on Pt(111) the formation of a weak Pt_3-H_β bond, which is responsible for the facile dehydrogenation on this surface. This bond is much weaker on both surface alloys, which partially explains the absence of dehydrogenation on Pt_3Sn/Pt(111) and Pt_2Sn/Pt(111).

The decrease of the adsorption energy of cyclopentene on the surface alloys compared to Pt(111) can be attributed to the changed electronic structure of the surface alloys and is, therefore, due to a *ligand effect*. The results show a great resemblance to the behavior of ethene on the same surfaces.[10,11] This suggests that, due to the similar bonding mechanisms, our results can also account for the chemisorption properties of ethene on the Pt_nSn(111) surface alloys. They are also related to the behavior of unsaturated aldehydes on the same surfaces.[6]

Acknowledgment. The authors gratefully acknowledge the financial support by the CNRS and the Deutsche Forschungsgemeinschaft through a bilateral research grant.

References and Notes

(1) Sachtler, W. H. M. *J. Mol. Catal.* **1984**, *25*, 1.
(2) Breitbach, J.; Franke, D.; Hamm, G.; Becker, C.; Wandelt, K. *Surf. Sci.* **2002**, *507−10*, 18.
(3) Paffett, M. T.; Gebhard, S. C.; Windham, R. G.; Koel, B. E. *Surf. Sci.* **1989**, *223*, 449.
(4) Batzill, M.; Beck, D. E.; Koel, B. E. *Surf. Sci.* **2000**, *466*, L821.
(5) Pick, S. *Surf. Sci.* **1999**, *436*, 220.
(6) Delbecq, F.; Sautet, P. *J. Catal.* **2003**, *220*, 115.
(7) Paffett, M. T.; Windham, R. G. *Surf. Sci.* **1989**, *208*, 35.
(8) Overbury, S. H.; Ku, Y.-S. *Phys. Rev. B* **1992**, *46*, 7868.
(9) Overbury, S. H.; Mullins, S. R. *Surf. Sci.* **1991**, *254*, 45.
(10) Paffett, M. T.; Gebhard, S. C.; Windham, R. G.; Koel, B. E. *Surf. Sci.* **1989**, *223*, 449.
(11) Tsai, Y.-L.; Xu, C.; Koel, B. E. *Surf. Sci.* **1997**, *385*, 37.
(12) Xu, C.; Peck, J. W.; Koel, B. E. *J. Am. Chem. Soc.* **1993**, *115*, 751.
(13) Xu, C.; Koel, B. E.; Paffett, M. T. *Langmuir* **1994**, *10*, 166.
(14) Xu, C.; Tsai, Y.-L.; Koel, B. E. *J. Phys. Chem.* **1994**, *98*, 585.
(15) Xu, C.; Koel, B. E. *Surf. Sci.* **1994** *304*, 249.
(16) Peck, J. W.; Koel, B. E. *J. Am. Chem. Soc.* **1996**, *118*, 2708.
(17) Tsai, Y.-L.; Koel, B. E. *J. Phys. Chem. B* **1997**, *101*, 2895.
(18) Peck, J. W.; Mahon, D. I.; Koel, B. E. *Surf. Sci.* **1998**, *410*, 200.
(19) Kresse, G.; Hafner, J. *Phys. Rev. B* **1993**, *47*, 558.
(20) Kresse, G.; Hafner, J. *Phys. Rev. B* **1993**, *48*, 13115.
(21) Kresse, G.; Hafner, J. *Phys. Rev. B* **1994**, *49*, 14251.
(22) Kresse, G.; Hafner, J. *Phys. Rev. B* **1998**, *59*, 1758.
(23) Perdew, J. P.; Wang, Y. *Phys. Rev. B* **1992**, *45*, 13244.
(24) Loffreda, D.; Jugnet, Y.; Delbecq, F.; Bertolini, J. C.; Sautet, P. *J. Phys. Chem. B* **2004**, *108*, 9085.
(25) Morikawa, Y. *Phys. Rev. B* **2001**, *63*, 033405.
(26) Avery, N. E. *Surf. Sci.* **1984**, *137*, L109.
(27) Avery, N. E. *Surf. Sci.* **1984**, *146*, 363.
(28) Henn, F. C.; Dalton, J. D.; Campbell, C. T. *J. Phys. Chem.* **1989**, *93*, 836.
(29) Redhead, R. A. *Vacuum* **1962**, *12*, 203.
(30) Abon, M.; Bertolini, J. B.; Billy, J.; Massardier, J.; Tardy, B. *Surf. Sci.* **1985**, *162*, 395.
(31) Tsai, M. C.; Mutterties, E. L. *J. Am. Chem. Soc.* **1982**, *104*, 2534.
(32) Villareal, J. R.; Laane, J.; Bush, S. F.; Harris, W. C. *Spectrochim. Acta A* **1979**, *35*, 331.
(33) Brizuela, G.; Castellani, N. J. *Surf. Sci.* **1998**, *401*, 297.
(34) Kimura, K.; Katsumata, S.; Achiba, Y.; Yamazaki, T.; Iwata, S. *Handbook of HeI Photoelectron Spectra of Fundamental Organic Molecules*; Halsted: New York, 1981.